Phosphorylation-Dependent Power Output of Transgenic Flies: An Integrated Study

Michael H. Dickinson,* Christopher J. Hyatt,# Fritz-Olaf Lehmann,* Jeffrey R. Moore,§ Mary C. Reedy,¶ Amanda Simcox,‖ Rutawain Tohtong,‖ Jim O. Vigoreaux,** Hiroshi Yamashita,§ and David W. Maughan§

*Department of Integrative Biology, University of California, Berkeley, California 94720; #Department of Medicine, Division of Cardiology, University of North Carolina, Chapel Hill, North Carolina 27599; §Department of Molecular Physiology and Biophysics, University of Vermont, Burlington, Vermont 05405; ¶Department of Cell Biology, Duke University, Durham, North Carolina 27710; ‖Department of Molecular Genetics, Ohio State University, Columbus, Ohio 43210; and **Department of Biology, University of Vermont, Burlington, Vermont 05405 USA

ABSTRACT We examine how the structure and function of indirect flight muscle (IFM) and the entire flight system of *Drosophila melanogaster* are affected by phosphorylation of the myosin regulatory light chain (MLC2). This integrated study uses site-directed mutagenesis to examine the relationship between removal of the myosin light chain kinase (MLCK) phosphorylation site, in vivo function of the flight system (flight tests, wing kinematics, metabolism, power output), isolated IFM fiber mechanics, MLC2 isoform pattern, and sarcomeric ultrastructure. The MLC2 mutants exhibit graded impairment of flight ability that correlates with a reduction in both IFM and flight system power output and a reduction in the constitutive level of MLC2 phosphorylation. The MLC2 mutants have wild-type IFM sarcomere and cross-bridge structures, ruling out obvious changes in the ultrastructure as the cause of the reduced performance. We describe a viscoelastic model of cross-bridge dynamics based on sinusoidal length perturbation analysis (Nyquist plots) of skinned IFM fibers. The sinusoidal analysis suggests the high power output of *Drosophila* IFM required for flight results from a phosphorylation-dependent recruitment of power-generating cross-bridges rather than a change in kinetics of the power generating step. The reduction in cross-bridge number appears to affect the way mutant flies generate flight forces of sufficient magnitude to keep them airborne. In two MLC2 mutant strains that exhibit a reduced IFM power output, flies appear to compensate by lowering wingbeat frequency and by elevating wingstroke amplitude (and presumably muscle strain). This behavioral alteration is not seen in another mutant strain in which the power output and estimated number of recruited cross-bridges is similar to that of wild type.

INTRODUCTION

Insect flight requires higher levels of mechanical power than any other form of animal locomotion. The high power output is thought to arise from morphological and physiological specializations of the insect flight muscles. In the present study we use *Drosophila melanogaster* to investigate the basis of the high power output.

In *Drosophila*, wing movement is powered by two antagonistic sets of indirect flight muscles (IFM) that are attached to the thoracic exoskeleton. The alternating contractions of the two sets of IFM deform the thorax and indirectly drive the wing movements. The IFM oscillate rapidly at nearly full filament overlap while asynchronous nerve impulses maintain an elevated level of intracellular Ca^{2+}. Although Ca^{2+} is a prerequisite for contraction, it is stretch that initiates the contraction that leads to oscillatory power production. Specifically, the delayed rise in muscle force following a quick stretch (denoted "stretch activation") in one set of IFM is initiated by a small extension caused by the contraction of the antagonist IFM.

Although stretch activation is, to some extent, a property of all striated muscles, the magnitude of stretch activation is especially prominent in muscles that power oscillatory systems (Pringle, 1949; Jewell and Ruegg, 1966; Steiger, 1977; Abbott and Steiger, 1977; Peckham et al., 1990; Zhao and Kawai, 1993; Gilmour and Ellington, 1993; Kawai et al., 1993). Various models have been postulated to explain the basis of stretch activation, including the model of Wray (1979). In the Wray model, a small lengthening improves the matching of actin targets and myosin cross-bridge arrays (but see Squire, 1992), resulting in a higher probability of attachment and thus an increase in force. More recently, Kawai and colleagues (Tawada and Kawai, 1990; Zhao and Kawai, 1993) have modeled stretch activation as a transition from a non-force-producing (weakly bound) cross-bridge state to a force-producing (strongly bound) state. In this type of model, transmission of strain to the thick filament affects strain-sensitive rate constants of the cross-bridge cycle and thus the distribution of cross-bridge states (Eisenberg and Greene, 1980; Thorson and White, 1983; Granzier and Wang, 1993b; Granzier and Wang, 1993a). The strain is transmitted by connecting filaments that link the thick filaments to the Z-lines (Granzier and Wang, 1993b), which in *Drosophila* consists of the molecule projectin (Saide et al., 1989). It has been postulated that IFM-specific proteins

Received for publication 19 December 1996 and in final form 10 September 1997.

Address reprint requests to David W. Maughan, Department of Molecular Physiology and Biophysics, University of Vermont, Burlington, VT 05405. Tel.: 802-656-4041; Fax: 802-656-0747; E-mail: maughan@salus.uvm.edu.

Authors are listed in alphabetical order except for D. Maughan.

0006-3495/97/12/3122/13 $2.00

(Bullard, 1983; Bullard et al., 1988; Vigoreaux et al., 1993) and/or a unique extension of the myosin regulatory light chain (MLC2) (Tohtong et al., 1995) may also play a role in enhancing stretch activation and power output in flies.

We showed recently (Tohtong et al., 1995) that *Drosophila* MLC2 has two conserved serines (amino acids 66 and 67) that are phosphorylated by myosin light chain kinase (MLCK). Because of *Drosophila* MLC2's unusual 54 amino acid extension of the N-terminus, the number of the conserved serines corresponds to positions 12 and 13 in chicken skeletal muscle MLC2 (Matsuda et al., 1977). Replacement of these serines by unphosphorylable alanines using site-directed mutagenesis attenuated the stretch activation response and oscillatory power output of the IFM, resulting in severe flight impairment. The overall sarcomeric structure of the IFM in the double mutant (denoted $Mlc2^{S66A,S67A}$) appeared to be normal by both optical and low magnification electron microscopy of thick sections, indicating that, though required for normal power output, phosphorylation is not required for myogenesis.

Powered flight is the end point in the chain of events starting with the interaction of actin and myosin. In the present study we extend the previous work by using an integrated approach to trace the power deficiencies in the MLC2 mutant flies from the molecular to the organismal level. Flight system power output was estimated from whole-animal respirometric and wingbeat kinematic measurements. IFM power output was estimated from sinusoidal length perturbation analysis of isolated skinned fibers, as described previously (Tohtong et al., 1995). Cross-bridge power output was estimated by implementing a mathematical model of sarcomere dynamics. We also examined the ultrastructure and MLC2 isovariant profile of the IFM at higher resolution than used previously. Our results suggest that a decrease in the constitutive level of MLC2 phosphorylation, without detectable disruption of sarcomere structure or cross-bridge derangement, decreases stretch activation and net power output of the IFM by reducing the number of attached cross-bridges rather than by changing the kinetics of the power-producing step of attached cross-bridges. $Mlc2^{S66A}$ and $Mlc2^{S66A,S67A}$ flies compensate for a reduced cross-bridge number and lower wingbeat frequency by elevating wingstroke amplitude (and presumable muscle strain). $Mlc2^{S67A}$ flies display little if any compensation since the number of recruited cross-bridges is similar to that of wild type. We conclude that MLCK-dependent phosphorylation of the *Drosophila* regulatory light chain is necessary for enhancing stretch activation and production of oscillatory power to meet the requirements of flight.

METHODS

Fly stocks and flight tests

Nucleotide sequences of the *Mlc2* gene encoding Ser-66 and/or Ser-67 were changed to Ala, and *P* element-mediated transformants containing the mutant *Mlc2* sequences ($Mlc2^{S66A}$, $Mlc2^{S67A}$, and $Mlc2^{S66A,S67A}$) were constructed using standard procedures (Kunkle et al., 1987). $Mlc2^{E38}$, a null mutation that truncates MLC2 at amino acid 10 (Warmke et al., 1992), served as the host strain. A control strain ($Mlc2^{+}$) was created by transforming $Mlc2^{E38}$ with two wild-type *Mlc2* genes. Several lines were generated for each transformed *Mlc2* gene (including four lines described previously (Tohtong et al., 1995), each with a different chromosomal *P* element insertion site. Fly stocks were maintained at 17°C on cornmeal-molasses-agar-based media. Crosses were performed at 25°C.

Individual 2- to 5-day-old female flies were tested for flight ability using a "Sparrow box" (Drummond et al., 1991; Tohtong et al., 1995). Wingbeat frequency was measured at room temperature using an "optical tachometer" (Hyatt and Maughan, 1994). Individual flies from each group, randomly selected, were dissected for either electron microscopy, protein analysis, functional tests of isolated IFM, or in vivo measurements of metabolic and mechanical power output.

Electron microscopy

Electron microscopy was used to evaluate the structure of wild-type and mutant IFM, both in the native state (fixed in the thorax) and in skinned (isolated) fibers. The skinned fibers were prepared in one of three states: MgATP-relaxed, Ca^{2+}-activated, or MgATP-free rigor (solutions 1–3, respectively; compositions given below). Details of the primary and secondary fixation protocols, staining and embedding methods, and thin sectioning procedures for high resolution electron microscopy are described elsewhere (Reedy et al., 1994).

Protein analysis

IFM were dissected from thoraces of adult flies and solubilized in IEF sample buffer (O'Farrell, 1975). Some flies were injected with ^{32}P (1 μl) and allowed to recover before dissection. Solubilized proteins were separated by two-dimensional polyacrylamide gel electrophoresis (2D-PAGE) and were either silver stained or stained with Coomassie Blue. Some gels were electroblotted on nylon membranes, followed by immunoblot analysis. Radioactive gels were exposed to x-ray film before immunoblot analysis. MLC2-specific antibodies were produced and Western hybridization conducted as described previously (Warmke et al., 1992). The in vivo MLC2 ^{32}P labeling, isolation, and analysis were performed according to standard methods (Vigoreaux and Perry, 1994). Gels were scanned with a densitometer (PDI, Huntington Station, NY) and quantified using commercial software (PDI's PDQUEST).

Isolated flight muscle fiber mechanics

Dorsal longitudinal IFM were dissected from split thoraces immersed for at least 1 h at 10–12°C in MgATP relaxing solution (solution 1) containing, in addition to the basic constituents listed below, 50% (w/v) glycerol and a detergent, either 0.5% (w/v) Triton X-100 or 100 μg/ml Saponin. The detergents solubilize cellular membranes, permitting equilibration of the bathing media with the interfilament space of the IFM (Maughan and Godt, 1989). Solution 1 contained 5 mM MgATP, 16 mM potassium phosphate, 15 mM phosphocreatine, 80 units/ml creatine phosphokinase, 1 mM free Mg^{2+}, 5 mM EGTA, and 0.11 mM $CaCl_2$ (yielding pCa 8 = $-\log[10^{-8}$ M $Ca^{2+}]$), 20 mM BES buffer (*N,N*-bis(2-hydroethyl)-2-aminoethanesulphonic acid, titrated to pH 7), 10 mM DTT, and 0.2 mM leupeptin. Ionic strength was adjusted to 175 mM with added potassium methane sulfonate. Solutions were formulated by solving a set of simultaneous equations describing the multiple equilibria of ions (Godt and Lindley, 1982).

The general experimental procedure has been described previously (Warmke et al., 1992). Briefly, a skinned fiber segment was transferred to a 20-μl drop of relaxing solution on the bottom of an 0.5-ml aluminum chamber filled with mineral oil (12 ± 0.5°C, temperature maintained by a Peltier device: Cambion, Cambridge Thermionic Corp., Cambridge, MA). The segment was attached via aluminum clips to tungsten hooks on a strain gauge (AE801, SensoNor, Horten, Norway) and piezoelectric motor (P173, Physik Instrumente GmbH and Co., Waldbronn, Germany). The relative

position of the motor head was monitored by a variable impedance displacement transducer (KD-2310, Kaman Instrumentation Corp., Colorado Springs, CO). Root-mean-square noise of the strain gauge was ~2 μN of the position detector, ~0.4 μm. The sensitivity of the strain gauge/hook was 1.63 mN/V; compliance, ~5 nm/μN; resonant frequency, 7.7 kHz. The compliance of the servomotor/hook was <1 nm/μN; −3 dB roll-off frequency, 600 Hz.

After the segment was stretched until just taut (zero stress), the distance between clips (L_o) was measured using a filar micromanometer and inverted compound microscope. Each fiber was stretched incrementally (by 2.5–5% steps), to a final strain of 1.05–1.15 L_o (corresponding to a fiber tension of ~1 kN m^{-2}, measured after "stress relaxation" (Granzier and Wang, 1993a). Fiber tension was obtained by dividing force by cross-sectional area (A), assumed circular. The width of the fiber in oil, measured at the narrowest part (generally the middle), was used for the diameter estimate (surface tension at the oil-water interface rounds the fiber). Mean segment length (wild type, 256 ± 21 um; mean ± SD) and diameters (wild type: 138 ± 4 um) were not significantly different between groups.

The skinned fibers were activated incrementally with Ca^{2+} by exchanging equal volumes of relaxing solution (solution 1: pCa 8) for Ca^{2+} activating solution (solution 2: pCa 4.5) to attain pCa of 7, 6, 5.5, 5, and 4.5. Activating solutions had the same ionic composition as relaxing solution, except 5.03 mM (pCa 4.5) instead of 0.11 mM $CaCl_2$ was added. Rigor was induced by exchanging activating solution for MgATP-free solution (solution 3: rigor) containing 0.11 mM $CaCl_2$, 5 mM EGTA, 20 mM BES buffer (pH 7.0), and 175 mM ionic strength (adjusted with potassium methane sulfonate). At the end of each experiment, each fiber was fixed for optical or electron microscopy by exchanging half the solution volume with rigor solution containing 1% (w/v) glutaraldehyde.

Sinusoidal analysis (Zhao and Kawai, 1993) was used to determine the dynamic viscoelastic characteristics and oscillatory power output of the skinned IFM during small amplitude length perturbations. The end of each fiber was oscillated at a specific frequency, and the resulting force response recorded. A set of responses from a strip of latex membrane (Trojan-enz, Carter-Wallace, NY) was recorded and used to obtain the system transfer function (Kawai and Brandt, 1980), which allowed the fiber data to be corrected for deviations in complex stiffness due to the experimental apparatus. The true complex stiffness of the muscle fiber, $y(f)$, was obtained from the expression: $y(f) = Y(f)\ R(f = 1\ \text{Hz})/R(f)$, where $Y(f)$ is the measured complex stiffness of the muscle fiber, $R(f)$ is the measured complex stiffness of the latex strip, and $R(f = 1\ \text{Hz})$ is the measured complex stiffness of the latex strip at 1 Hz, a frequency at which the error introduced by the system is negligible.

Digitized length and force signals from the servomotor and strain gauge were used to calculate the elastic and viscous components of the complex stiffness $y(f)$ by computing the amplitude ratio and the phase difference for the change in tension and length at each frequency. Anti-aliasing and noise reduction in the sampled force and length signals were provided by a pair of matched low-pass analog filters (6-pole Bessel). Complex stiffness moduli ($y(f)\ L_o$/A) were plotted as Nyqvist diagrams, where the abscissa and ordinate of the diagram represent the elastic and viscous components (Kawai and Brandt, 1980).

Wingbeat kinematics and metabolic measurements

In vivo tests were conducted on flies tethered in a cylindrical "virtual reality" flight arena equipped with a flow-through respirometry chamber (Dickinson and Lighton, 1995; Lehmann and Dickinson, 1997). The visual arena consisted of 1536 independently controlled green LEDs, each representing ~5° of visual arc. Flies were anesthetized and tethered with light-activated adhesive to a thin tungsten wire, the free end of which was attached to a force transducer (Lehmann and Dickinson, 1997). The transducer measured the force parallel to the animal's longitudinal body axis, and the total flight force was reconstructed trigonometrically by assuming that the total force vector was oriented at an angle of 24° with respect to the longitudinal body axis (Gotz and Wandel, 1984). During hovering and slow forward flight, the longitudinal body axis is oriented at 60° with respect to the horizontal plane (David, 1978; Dickinson and Gotz, 1996), so that the total flight force vector is roughly normal to the horizontal plane (sine of 24° + 60° = sin 84°). The force transducer was fixed inside a 20-ml respirometry chamber, into which room air (scrubbed of CO_2 and water) was pulled at 200 ml/min. The CO_2 content of the chamber was measured using a calibrated gas analyzer (Lighton, 1991). Instantaneous frequency and amplitude of the wingstroke were measured using an optical wingbeat analyzer (Gotz, 1987). Four channels of data (flight force, CO_2 production, wingbeat frequency, and stroke amplitude) were sampled at 8.3 Hz using a digital converter and data acquisition software (Axotape, Axon Instruments, Foster City, CA) and stored for subsequent analysis.

All experiments were performed under closed-loop conditions in which the flies could actively orient to a 20° vertical dark stripe by modulating the relative stroke amplitude of their two wings (Gotz, 1987; Dickinson and Lighton, 1995; Lehmann and Dickinson, 1997). While the flies were actively controlling the position of the stripe in the horizontal plane, a background pattern of diagonal lines was moved up and down in the vertical direction. The digital design of the visual display allowed the vertical stripe and the background pattern to move independently. The flies responded to the vertical oscillations of the background by modulating the magnitude of their total flight force. At the end of each flight sequence, the net metabolic cost of flight (P^*_{CO2}) was calculated by subtracting the resting CO_2 signal from the CO_2 signal measured during flight. These values of net CO_2 production were calibrated as metabolic rates assuming catabolism of carbohydrates with a respiratory quotient of 1.0 (Lighton, 1991; Lehmann and Dickinson, 1997).

Using wingstroke frequency, amplitude, and a number of morphological parameters, we used the equations of Ellington (1984) to calculate the instantaneous inertial and aerodynamic power at each sampled point within the flight sequence. As has been described previously (Dickinson and Lighton, 1995; Lehmann and Dickinson, 1997), elastic storage within the flight motor is sufficient to negate the contribution of inertial power, so that the total mechanical power (P^*_{mech}) requirements are equal to the aerodynamic power costs alone (Ellington, 1984). The muscle efficiency of the IFM, defined as the ratio of mechanical output to metabolic input, was calculated from the ratio of P^*_{mech} and P^*_{CO2}.

RESULTS

Removal of the MLCK-dependent phosphorylation sites does not affect myofibrillar ultrastructure

Myofibrillar and sarcomeric structures of IFM from all four transformant strains (*Mlc2*$^+$, *Mlc2*^{S66A}, *Mlc2*^{S67A}, and *Mlc2*^{S66A,S67A}) appeared normal, consistent with the previous report (Tohtong et al., 1995). For example, *Mlc2*^{S66A,S67A}, which has the most extreme functional phenotype, had sarcomeres that were well demarcated by Z lines, with average sarcomere lengths (3.01 ± 0.14 μm) and number of thick filaments across the diameter of the myofibrils (33.0 ± 1.2) that were not significantly different from those of *Mlc2*$^+$ (3.22 ± 0.55 μm, 34.5 ± 0.8) or wild type (2.94 ± 0.05 μm, 35.5 ± 1.0).

To determine whether subtle structural disruptions exist at the level of individual cross-bridges, we examined ultrathin sections of IFM from mutant and control flies. IFM fibers fixed in the rigor state (Fig. 1, *c* and *f*) showed well-ordered cross-bridge arrays in all lines examined. Precisely aligned, angled doublet groups were visible every 38 nm along the actin filament, similar to that observed in *Lethocerus* (Reedy et al., 1994). Fig. 1 *a* and *d* compares

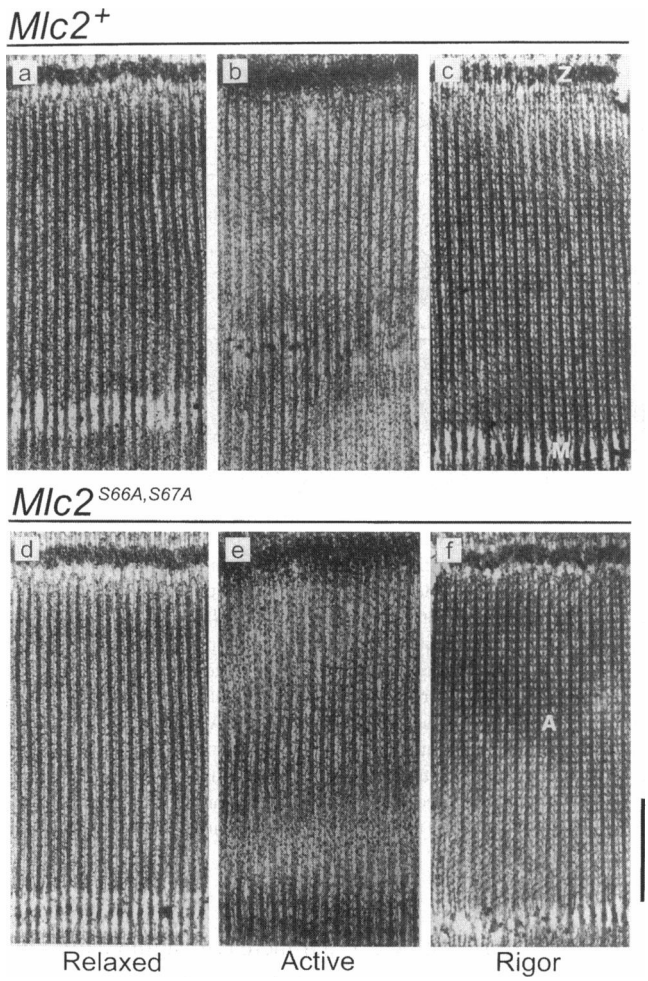

FIGURE 1 Ultrastructure of IFM from homozygous *Drosophila* MLC2 null mutants transformed with wild (*a–c*, line *JW1*) and mutant (*d–f*, *R3T1*) MLC2 genes. Relaxed (*a, d*), Ca^{2+}-activated (*b, e*), and rigor (*c, f*) fibers fixed in situ in the thorax. Longitudinal 25-nm sections, showing a little over one-half sarcomere (Z, Z-line; *M*, M-line; *A*, A-band). Note the very short I-band regions (containing thin filaments and projectin) versus the long A-band (containing both thin and thick filaments). Both $Mlc2^{+}$ and $Mlc2^{S66AS67A}$ cross-bridges are similarly well-ordered and respond appropriately to the presence or absence of ATP. Bar = 0.5 um.

ATP-relaxed states from control ($Mlc2^{+}$) and double serine substitution mutant flies ($Mlc2^{S66A,S67A}$). Both longitudinal sections of ATP-relaxed fibers display 14.5 nm periodic collars on the thick filaments as well as numerous thin bridging densities intersecting the thin filament at various axial angles centered around 90°. Ca^{2+}-activated fibers from $Mlc2^{S66A,S67A}$ mutant flies were also indistinguishable from those of the $Mlc2^{+}$ control (Fig. 1, *b* and *e*).

Phosphorylation generates multiple MCL2 isovariants

In *Drosophila*, *Mlc2* is a single copy gene which encodes a single protein (Parker et al., 1985; Toffenetti et al., 1987). We used 2D-PAGE with a shallow pH gradient that helped resolve the individual isovariants of MLC2 in IFM. A Western blot of wild-type IFM incubated with an anti-MLC2 polyclonal antibody is shown in Fig. 2 *a*. The antibody recognized ~14 protein spots that separated into two categories: eight variants at ~31 kD and six variants at ~33 kD. The apparent values are considerably higher than the calculated ~24-kD values (Parker et al., 1985), suggesting a tertiary structure whose presence in SDS retards mobility. Spot N1 corresponds to the major product of a MLC2 cDNA transcribed and translated in vitro (our unpublished observation). Spot N1 is not labeled with radioactive phosphate when $^{32}PO_4$ is injected into adult fly thoraces (Fig. 2, *d–f*), suggesting N1 corresponds to the unphosphorylated primary translation product of the MLC2 gene. All other MLC2 spots are labeled in vivo with ^{32}P. Spot P1, in particular, co-migrates with the major in vitro phosphorylated product (data not shown) obtained when recombinant MLC2 is incubated with rabbit recombinant MLCK (gift of James Stull, University of Texas). From these results we conclude *Drosophila* IFM contains ~14 antigenically related variants of MLC2, 13 of which are phosphorylated in the adult IFM.

Substitution of MLCK-phosphorylated serines with alanines increases accumulation of nonphosphorylated MLC2 in flight muscles

Using the higher-resolution gel system, we reexamined the change in MLC2 isoform pattern with phosphorylation site removal, using the wild type, control, and mutant lines examined previously. The mutants exhibited differences in the levels of nonphosphorylated versus phosphorylated isovariants, especially when compared with control $Mlc2^{+}$ IFM (Fig. 2 *e*), which produced gel patterns indistinguishable from wild type (Fig. 2 *d*). The most dramatic difference was in $Mlc2^{S66A,S67A}$, where we detected a 3- to 10-fold increase in the accumulation of the unphosphorylated variant compared to control (compare spots N1 in Fig. 2, *b* and *c*). The increase in relative abundance of N1 was accompanied by a decrease in the ratio of the phosphorylated spots P1a to P1b (compare Fig. 2, *e* and *f*). Specifically, the P1a/P1b ratio of $Mlc2^{S66A,S67A}$ was ~10-fold less than that of $Mlc2^{+}$, and this decrease was accompanied by a reduced accumulation of the most acidic isovariants (*arrowheads* in Fig. 2, *b* and *c*). An extreme example is shown in Fig. 2, *e* and *f*, where the two most acidic spots of the slow migrating series (*arrows*) are completely missing. Comparison of densities of protein stains from wild-type and MLC2 mutant flies suggest that ~25% of the native protein is phosphorylated by MLCK, and ~70% is phosphorylated by other kinases whose identities have yet to be determined.

MLCK-dependent phosphorylation site removal attenuates power output of isolated IFM fibers

To determine the direct effects of the MLC2 mutations on IFM power output and the underlying cross-bridge pro-

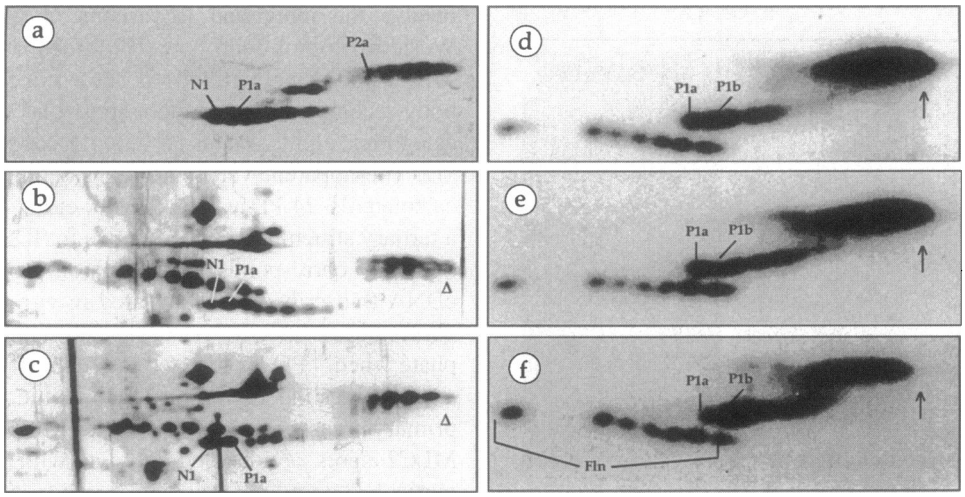

FIGURE 2 Two-dimensional gel electrophoretic analysis of regulatory myosin light chain phosphorylation from wild-type ($Mlc2^{+}$: line *JW*[60.1]) and mutant ($Mlc2^{S66A,S67A}$: line *R3T1*) flies. All samples represent proteins extracted from dissected indirect flight muscle fibers. (*a*) Immunoblot analysis from wild-type IFM. Approximately 14 isoelectric variants that separate into two distinct molecular weight classes are detected with this polyclonal antibody. The spot labeled N1 co-migrates with spot 148 of Mogami et al. (1982) and with the in vitro translated product of an $Mlc2^{+}$ cDNA. Spot P1a co-migrates with the major in vitro phosphorylated product when recombinant wild-type MLC2 is incubated with rabbit recombinant MLCK. Spot P2a co-localizes with Mogami et. al. (1982) spot 138. (*b*) Silver stained gel from control $Mlc2^{+}$ IFM (null rescued with two copies of the wild-type gene). The MLC2 protein pattern is indistinguishable from wild-type. (*c*) Silver stained gel from $Mlc2^{S66A,S67A}$. Note the marked increased in intensity of spot N1 relative to adjoining spot P1a. In addition, the most acidic slow-migrating phosphovariant (indicated by an *arrowhead*) is reduced in this mutant. (*d*) Autoradiogram of labeled phosphoproteins after injection of $^{32}PO_4$ into wild-type adult flies. Superimposing the autoradiogram onto its corresponding immunoblot showed that all MLC2 isovariants with the exception of N1 are phosphovariants. (*e*) Autoradiogram of MLC2 phosphoproteins from $Mlc2^{+}$. The pattern is indistinguishable from wild-type. (*f*) Autoradiogram of MLC2 phosphoproteins from $Mlc2^{S66A,S67A}$. Note that the relative accumulation of P1a and P1b is different from that seen in $Mlc2^{+}$. Furthermore, the most acidic slow-migrating phosphovariant (indicated by an *arrow*) is reduced in this mutant, consistent with panel *c*. "Fln" correspond to flightin phosphovariants (Vigoreaux and Perry, 1994).

cesses, we conducted mechanical tests on Ca^{2+}-activated skinned fibers isolated from flies of the mutant and wild-type strains used above. The individuals tested produced flight indices (Table 1) that were similar to the group flight indices reported previously (Tohtong et al., 1995).

IFM steady-state isometric tension

Fig. 3 shows pCa-tension relationships of skinned IFM fibers isolated from each line. In general, steady-state tension began to rise at pCa 7 and increased sigmoidally with calcium concentration to reach a maximum at ~pCa 5. We fitted Hill curves to the data by least squares as shown in Table 2. No significant differences ($p > 0.1$) were observed among strains in either pCa_{50} (the calcium concentration at which 50% of maximum isometric tension is developed) or T_{max} (the maximum isometric force per unit cross-sectional area). In contrast, a reduction in Hill coefficient (or cooperativity index) was observed in some serine mutants [mean differences were either significant ($Mlc2^{S67A}$, $p < 0.05$); on the borderline of significance ($Mlc2^{S66A}$, $p = 0.06$); or not significant ($Mlc2^{S66A,S67A}$, $p > 0.01$)].

TABLE 1 Flight indices and wingbeat frequencies of flies used for the isolated IFM skinned fiber experiments

Strain	Number (*n*)	Flight Index (0–6)	Wingbeat Frequency (s^{-1})
Wild type	7	5.8 ± 0.1	206 ± 7
$Mlc2^{+}$	7	5.4 ± 0.8	213 ± 4
$Mlc2^{S67A}$	5	5.4 ± 0.9	207 ± 7
$Mlc2^{S66A}$	6	3.0 ± 1.0*	177 ± 3*
$Mlc2^{S66A.S67A}$	6	0.9 ± 0.6*	152#

Means ± S.E.M.
*$p < 0.05$ versus $Mlc2^{+}$.
#Only one of the six flies tested could be induced to beat its wing. Flight index determined using the "Sparrow box" (Drummond et al., 1991). Wingbeat frequency determined using an "optical tachometer" (Hyatt et al., 1994). Difference between $Mlc2^{S67A}$, $Mlc2^{+}$, and *wild type* not significant ($p > 0.1$). Lines used: *Canton S, JW[60.1], R2T2, R1T3*, and *R3T1* (top to bottom).

Sinusoidal analysis

A typical Nyquist plot for a skinned fiber in the relaxed, active, and rigor states is shown in Fig. 4 for a wild-type fly. The frequency-dependent complex stiffness moduli were least in the relaxed state (pCa8) and greatest in the rigor state (no MgATP). In the Ca^{2+}-activated state (pCa 4.5), the fiber exhibited a marked increase in negative viscous modulus ($-E_v$), which resulted in a loop. A negative viscous modulus indicates the fiber performs mechanical work on the apparatus driving the oscillatory changes. Maximal mechanical work is proportional to the maximum value of the negative viscous modulus ($|-E_v|$).

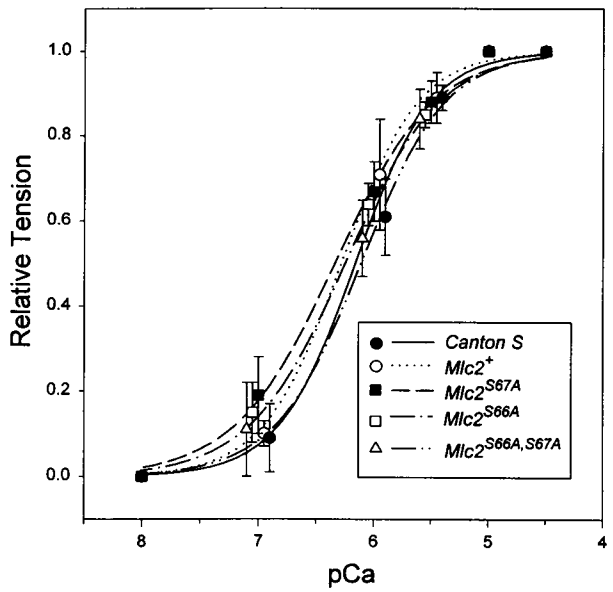

FIGURE 3 pCa-tension relation of mutant IFM versus wild-type. Curves were fit by least squares to the equation $T_x/T_{max} = x^n/(a^n + x^n)$, where T_x is the isometric tension at $[Ca^{2+}] = x$ (in molar), T_{max} is the maximal isometric tension (pCa 4.5 = $-\log(3.16 \times 10^{-5}$ M)), $a = [Ca^{2+}]$ at half-maximal tension ($pCa_{50} = -\log a$), and n is the Hill coefficient (cooperativity index). Temperature, 12°C.

Fig. 5 (*left panels*) shows Nyqvist plots of other Ca^{2+}-activated skinned IFM fibers that exhibit graded reductions of loop size with progressive removal of the phosphorylation sites. The maximum value of $|-E_v|$ for $Mlc2^+$ was not significantly different from that of wild-type (Tohtong et al., 1995). $Mlc2^{S66A}$ and $Mlc2^{S66A,S67A}$, but not $Mlc2^{S67A}$, exhibited significant, graded reductions in $|-E_v|$ compared to controls, indicating oscillatory work output is affected primarily by the S66A phosphorylation site mutation, with the reduction exacerbated by the double mutation.

Viscoelastic model of IFM fiber and power measurements

To help interpret our results in the context of changes in cross-bridge recruitment and kinetics, we modeled the viscoelastic properties of the skinned IFM fiber as three composite elements (*A*, *B*, and *C*), each contributing a component to the total dynamic stiffness. The combined dynamic stiffness, $y(f)$, over the experimental range of frequencies (f = 0.5–1000 Hz) can be expressed as the sum of the Fourier transforms representing each component:

$$y(f) = A(if/\alpha)^k - B\, if/(b + if) + C\, if/(c + if), \quad (1)$$

where $i = (-1)^{1/2}$, α is a constant (= 1 Hz, by definition), and k is a unitless exponent proportional to the phase angle of the Nyqvist plot. The coefficients A, B, and C (N m^{-2}) represent the magnitudes of *A*, *B*, and *C*, respectively. Frequencies b and c (s^{-1}) are *characteristic frequencies* of *B* and *C*.

The sum of all three terms reflect properties of *passive* myofibrillar elements, lumped as a nonexponential component *A*, in parallel with *active* MgATP-dependent cross-bridge elements represented by two exponential components *B* and *C*. Components *B* and *C* possess distinctly different characteristic frequencies and phase relationships. Component *A* represents the combined viscoelastic properties (i.e., frequency-dependent changes in composite stiffness) of several structural elements, including the elongated protein projectin that connects the thick filament to Z-line proteins (Saide et al., 1989). The magnitude of A reflects the extent to which these passive elements contribute to the dynamic stiffness of the fiber. Components *B* and *C*, which produce the Nyquist loops, represent the active properties of the actomyosin cross-bridges; i.e., the frequency-dependent changes in cross-bridge stiffness arising from strain-induced transitions between cross-bridge states, as mentioned previously (also see Discussion). The magnitudes of B and C reflect the number of power-producing cross-bridges, as well as the magnitude of their unitary stiffness moduli. Components *B* and *C* are essentially absent at very low concentrations of Ca^{2+} (resting) or $MgATP^{2-}$ (rigor), resulting in roughly linear Nyquists (Fig. 4, pCa 8 and rigor). At higher $[Ca^{2+}]$ and $[MgATP^{2-}]$, *B* and *C* are present, resulting in looped Nyquists (Fig. 4, pCa 4.5).

An important assumption underlying this representation of dynamic stiffness is that component *A* in the relaxed, active, and rigor states differs in magnitude but not in form. That is, over the experimental range of frequencies, the relaxed and rigor data fall roughly along a straight line with approximately the same slope (Fig. 4). The similarity of form in the presence of 30 mM 2,3-butanedione monoxime, which sharply reduces the number of attached cross-bridges (Zhao and Kawai, 1994), support this interpretation (our unpublished results). These observations motivated our use of the Fourier term $A(if/\alpha)^k$ to characterize *A*, which plots as a straight line through the origin in the Nyquist plot, with the slope determined by k (Fig. 4). The time course of *A* in response to a stepwise increase in fiber length is an abrupt increase in force (simultaneous with the length change) followed by a nonexponential decay.

A two-step iterative, least-squares curve-fitting routine similar to one described elsewhere (Kawai and Brandt,

TABLE 2 Isometric tension as a function of calcium concentration in skinned IFM of wild-type and mutant flies

Strain	*n*	pCa_{50}	Hill coefficient	T_{max}
Wild type	7	6.2 ± 0.1	1.4 ± 0.1	3.2 ± 0.4
$Mlc2^+$	7	6.3 ± 0.1	1.3 ± 0.1	2.4 ± 0.3*
$Mlc2^{S67A}$	6	6.3 ± 0.1	1.0 ± 0.1*	2.3 ± 0.2
$Mlc2^{S66A}$	6	6.3 ± 0.1	1.1 ± 0.1#	2.5 ± 0.2
$Mlc2^{S66A,S67A}$	6	6.1 ± 0.1*	1.2 ± 0.2	2.2 ± 0.3#

Means ± S.D. Temperature, 12°C. Same lines used as in Table 1. T_{max} is the maximal isometric tension (pCa 4.5) and pCa_{50} is the pCa at half-maximal tension. Parameters were returned from a least squares fit to the equation: $T_x/T_{max} = x^n/(a^n + x^n)$, where T_x is the isometric tension at $[Ca^{2+}] = x$ (in molar), $a = [Ca^{2+}]$ at half-maximal tension ($pCa_{50} = -\log a$), and n is the Hill coefficient (cooperativity index).

*$p < 0.05$ versus *wild type*.

#$p < 0.05$ versus $Mlc2^+$; other comparisons not significantly different.

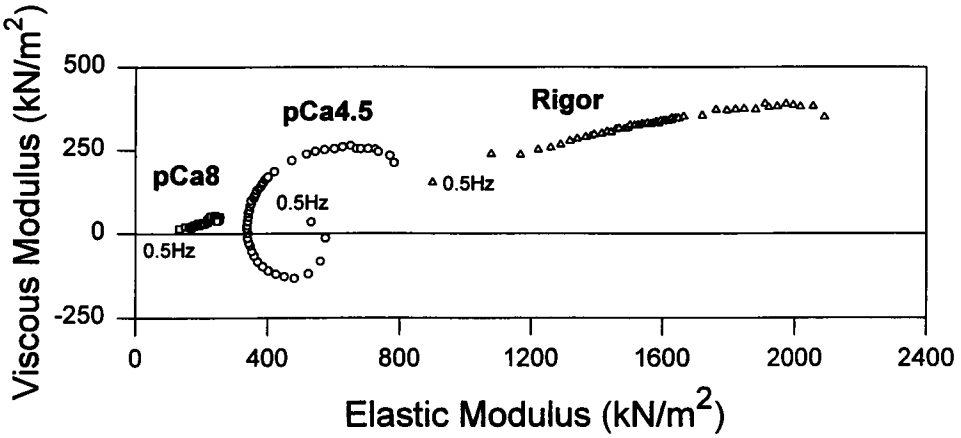

FIGURE 4 Nyquist plots of wild-type IFM in relaxed (pCa 8), activated (pCa 4.5), and rigor states. Dynamic stiffness modulus measured at 47 sinusoidal frequencies, progressing from 0.5 Hz to 1 kHz (left-to-right and clockwise). A list of frequency values and other parameters used for the signal processing (D/A sampling rates, D/A steps per cycle, A/D sample points per cycle, A/D number of cycles, A/D sampling rates, A/D delay periods) is available upon request.

1980) was used to fit $y(f)$ to the Nyquist plots. The value of k returned from relaxed, active and rigor fiber fits was not significantly different ($p < 0.05$; data not shown). Equation 1 fitted all data with a <4% deviation in root-mean-square value from the fitted means.

Table 3 compares model parameters of transformant flies and wild-type Ca^{2+}-activated skinned IFM fibers. Examples of deconvoluted Nyquists of processes *A*, *B*, and *C* are given in the right panel of Fig. 5, where the sum of all three $y(f)$ is plotted as the continuous curve through the data points in the corresponding Nyquist on the left. The $Mlc2^{+}$ and $Mlc2^{S67A}$ model parameters (Table 3) were not significantly different from those of wild-type ($p > 0.1$), although B and C values tended to be lower (see also right panels, Fig. 5). In contrast, $Mlc2^{S66A}$ and $Mlc2^{S66A,S67A}$ showed appreciable reductions of some parameters (A, B and C), but not of others (*b*, *c* and *k*). Notably, the values of B and C, reflecting the number of recruited cross-bridges, were significantly less ($p < 0.05$) in both strains compared to wild-type. The values were least in $Mlc2^{S66A,S67A}$. In contrast, the values of *b* and *c*, reflecting the kinetics of the cross-bridges, were not significantly different ($p > 0.1$).

MLCK-dependent phosphorylation site removal reduces in vivo mechanical power output

To better understand the relationship between flight impairment (reduced flight system performance) and the deficit in oscillatory power output of isolated IFM, we examined the power output of whole animals. Muscle performance was assessed by measuring the wingbeat frequency, wingbeat amplitude, flight force, and metabolic rate of each fly in the flight arena. From these measurements, metabolic power output, mechanical power output, and muscle efficiency were calculated.

Results of the arena experiments are given in Table 4, where visually induced modulations in total force production were used to compare the flight performance of wild-type and mutant flies under *peak* and *hovering* conditions (Lehmann and Dickinson, 1997). While all wild-type (*Canton S*) and rescued ($Mlc2^{+}$) flies could generate sustained flight within the arena, some of the mutants tested could not. Flight impairment was greatest in $Mlc2^{S66A,S67A}$, where only 2 or 3 of 7 individuals tested could fly in the arena. However, while not all mutant flies could fly in the arena, the flight duration of those that did fly was normal. Mean flight duration of fliers averaged over all mutant phenotypes was 18 ± 11 min, compared to 18 ± 6 min for wild-type flies.

The data shown in the table for peak performance derive from portions of the flight records in which the flies generated forces within 1% of their maximal values. Wild-type and control flies were capable of producing maximum forces of ~135% of body weight with a metabolic power output of nearly 700 W/Kg (muscle mass), similar to that reported previously (Lehmann and Dickinson, 1997). Compared with *Canton S* values, maximum force produced by the three mutant lines was significantly less (72–81%, $p < 0.05$), as was metabolic power output (67–84%, $p < 0.05$). Mechanical power (roughly proportional to the cube of both stroke frequency and stroke amplitude (Weis-Fogh, 1973), was also significantly lower in all three mutant lines (68–85%, $p < 0.05$). The lower metabolic rate in the mutants correlated with the decrease in mechanical power output and not an increase in efficiency. Muscle efficiency during peak force production was ~10% in both mutant and wild-type flies, whereas mechanical power output was significantly lower in all three mutant lines. In $Mlc2^{S66A}$ and $Mlc2^{S66A,S67A}$ the decrease in maximum mechanical power was due primarily to a drop in frequency but not in amplitude. However, in $Mlc2^{S67A}$ the situation was reversed, such that the drop in maximum mechanical power was due to a decrease in stroke amplitude while stroke frequency remained at wild type levels. No significant difference in force or power was observed between the control lines (*Canton S* and $Mlc2^{+}$).

For flight system performance assessed under *hovering* conditions, the flies produced a total flight force just equal to body weight. The mechanisms by which the mutants generated hovering forces were quite different from those of *Canton S* and $Mlc2^{+}$. In both $Mlc2^{S66A}$ and $Mlc2^{S66A,S67A}$ the total metabolic cost of hovering flight was significantly

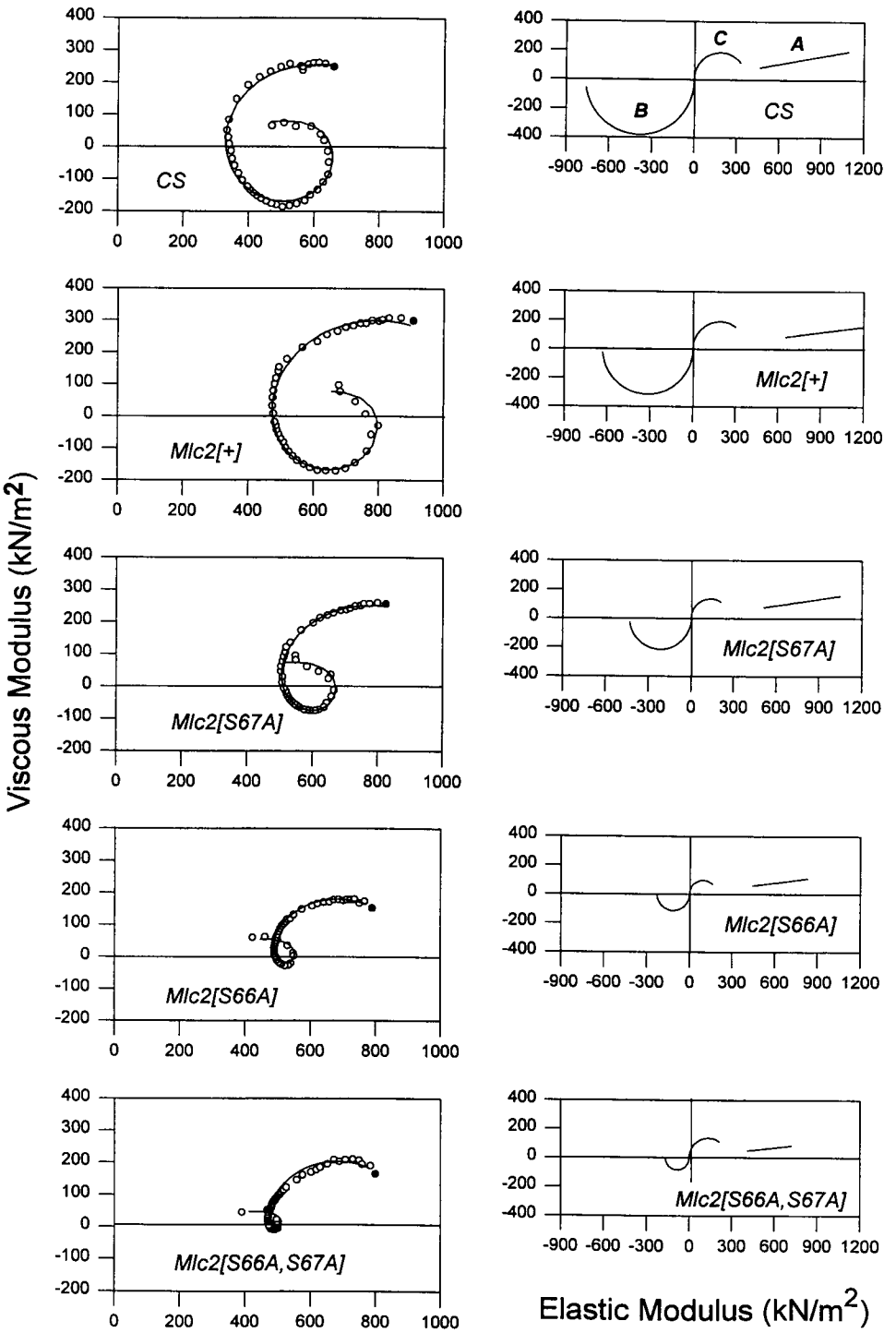

FIGURE 5 Nyquist plots of mutant versus control IFM in the activated state (pCa 5). Left-hand panels: skinned fiber data points corresponding to sinusoidal frequencies from 0.5 Hz (indicated) to 1 kHz. Right-hand panels: deconvolution of data according to Eq. 1. Curves: least squares fits to Eq. 1. Parameter values are included in the pooled results presented in Table 3. Note the pronounced gradation of the amplitudes of maximum negative viscous moduli. The corresponding elastic moduli (at the frequency of maximum negative viscous modulus of the active state, f_{max}) were not significantly different among strains ($p > 0.1$). In the relaxed (pCa 8) or rigor states, the values for the viscous and elastic moduli at f_{max} were not significantly different among strains ($p > 0.1$; data not shown). Temperature, 12°C.

less that of the control. Thus, total flight efficiency (flight force divided by P^*_{CO2}) was much greater. Since muscle efficiency within these flies did not increase significantly, these results are most likely explained by an increase in aerodynamic performance. In short, these mutants generated greater flight force for a given stroke frequency and amplitude. Although somewhat puzzling, variations in aerodynamic performance are not entirely unexpected because flies are capable of voluntarily modulating force generation by regulating non-steady-state aerodynamic mechanisms (Lehmann and Dickinson, unpublished observation). The mutant fliers may have compensated for a loss of muscle power by changing stroke kinematics to increase aerodynamic force production.

The rough correlation between oscillatory power output of the fly's flight system (Table 4) and constituent IFM (Table 3) is consistent with the graded effect of MLCK-dependent phosphorylation site removal on cross-bridge

TABLE 3 Model parameters and power outputs of Ca^{2+}-activated (pCa 5) skinned IFM of wild-type and mutant flies

Strain	n	A (kN m^{-2})	B (kN m^{-2})	C (kN m^{-2})	k	b (s^{-1})	c (s^{-1})	P_B (W m^{-3})	P_{IFM} (W m^{-3})
Wild type	7	348 ± 42	407 ± 59	313 ± 33	0.09 ± 0.01	53.7 ± 13.5	439 ± 50	111 ± 37	24 ± 7
Mlc2^{+}	7	438 ± 45	412 ± 51	272 ± 36	0.09 ± 0.01	45.3 ± 3.9	479 ± 61	94 ± 14	22 ± 4
Mlc2^{S67A}	6	368 ± 33	353 ± 22	281 ± 18	0.08 ± 0.01	64.5 ± 7.0	409 ± 45	114 ± 13	17 ± 2
Mlc2^{S66A}	6	308 ± 45*	249 ± 36*#	165 ± 15§¶	0.09 ± 0.01	54.1 ± 6.5	404 ± 37	68 ± 11§¶	11 ± 2§
Mlc2^{S66A,S67A}	6	253 ± 42*	166 ± 27§¶	132 ± 30§¶	0.10 ± 0.01	56.0 ± 7.3	367 ± 40	47 ± 10§¶	2 ± 0.4§

Means ± S.E.M. Same lines used as in Table 1. See Eq. 1 for definition of model parameters A, B, C, k, b, and c. Values of k were not significantly different ($p > 0.1$) among strains. P_B is defined as the total oscillatory power output of the crossbridges, where $P_B = \pi B b (\Delta L/L)^2$ (Tohtong et al., 1995). B is the amplitude (kN/m^2), b is the characteristic frequency (s^{-1}) of the crossbridge work-generating process *B* (Eq. 1), *L* is the fiber length between the attachment clips and $\Delta L/L$ is the ratio of the half amplitude of the length perturbation divided by *L* (= 0.00125 for the experiments listed). P_{IFM} is the net oscillatory power delivered by the IFM to the apparatus (flight system), where $P_{IFM} = \pi E_v f(\Delta L/L)^2$. E_v is the viscous modulus (kN/m^2) and *f* is the frequency of the length perturbation (s^{-1}). The values of P_{IFM} listed here are values at which the product of E_v and *f* is maximum. In the fly, P_{IFM} is the product of the wingbeat frequency and the net work per stroke after part of the total work produced by the crossbridges has been dissipated as heat.
*$p < 0.05$ versus *Mlc2*$^{+}$.
#$p < 0.05$ versus wild type.
§$p < 0.01$ versus wild type.
¶$p < 0.01$ versus *Mlc2*$^{+}$.

recruitment and muscle performance. The reduced mechanical power output of *Mlc2*^{S66A} and *Mlc2*^{S66A,S67A} correlates with a reduction in wingstroke frequency. Note, however, wingstroke amplitude of the hovering fly was slightly elevated during hovering flight, suggesting these flies may have attempted to compensate for a drop in stroke frequency by increasing the amplitude. In contrast, the hovering performance of *Mlc2*^{S67A} was similar to wild type (with the exception of a slight decrease in stroke amplitude).

DISCUSSION

This report extends a previous study of *Drosophila* flight muscle in which the MLCK-dependent phosphorylation sites, serines 66 and 67 of the regulatory light chain, substituted by unphosphorylatable alanines, produced flight impairment (Tohtong et al., 1995). The present results reveal which aspects of IFM structure and function contribute to the impairment, and how the flight system as a whole compensates for reductions in power output of the IFM fibers.

Normal IFM ultrastructure, altered MLC2 isovariant profile

Rigor, active, and ATP-relaxed mutant cross-bridge arrays revealed no structural alterations that could account for the loss of power output and flight impairment. In Ca^{2+}-activated IFM, the sarcomere pattern (Z lines and M bands) remained intact despite some sarcomere shortening, indicating that the organization of the mutant myofibrils was robust. This result is in accord with the similarity in amplitude of Ca^{2+}-activated isometric tension of isolated mutant and control IFM. It is still possible that *subtle* structural

TABLE 4 Flight performance during *peak* and *hovering* conditions

Condition	Genotype	*n*	Force/wt	Frequency (Hz)	Amplitude (degs)	P^*_{mech} (W/Kg)	P^*_{CO2} (W/Kg)	Efficiency (%)
Peak	*Wild type*	10/10	1.35 ± 0.18	207 ± 1.2	170 ± 3	80 ± 13	695 ± 103	9.7 ± 1.1
	Mlc2^{+}	7/7	1.35 ± 0.18	207 ± 10	171 ± 5	72 ± 8	687 ± 98	9.3 ± 0.8
	Mlc2^{S67A}	7/7	1.10 ± 1.14*	205 ± 15	159 ± 8*	68 ± 8#	478 ± 19§	10.3 ± 1.3
	Mlc2^{S66A}	6/8	1.08 ± 0.22#	179 ± 13*	173 ± 5	54 ± 12§	463 ± 95§	10.1 ± 0.8
	Mlc2^{S66A,S67A}	3/7	1.03 ± 0.19#	168 ± 3§	172 ± 2	55 ± 0§	574 ± 66#	9.9 ± 0.3
Hovering	*Wild type*	10/10	1.0	205 ± 15	161 ± 6	68 ± 10	639 ± 85	9.0 ± 1.0
	Mlc2^{+}	7/7	1.0	201 ± 16	163 ± 3	58 ± 7	592 ± 113	8.7 ± 1.1
	Mlc2^{S67A}	4/7	1.0	206 ± 16	151 ± 3*	63 ± 7	582 ± 44	9.0 (1)
	Mlc2^{S66A}	4/8	1.0	189 ± 19	164 ± 11	53 ± 7*	488 ± 62*	9.7 ± 1.1
	Mlc2^{S66A,S67A}	2/7	1.0	169 ± 2§	168 ± 2#	52 ± 1§	474 ± 8§	9.6 ± 0.1

Means ± S.D. Same lines used as in Table 1. Listed are values of flight performance obtained at maximum flight force (*Peak*) and during that portion of flight where flight force just equals body weight (*Hovering*). Force/weight: ratio of maximum force to body weight. Wingbeat frequency and stroke amplitude: self explanatory. P^*_{mech}: mechanical power output (W/Kg), calculated from detailed kinematics and body morphology, assuming muscle mass is equal to 30% of body weight. $P^*_{CO_2}$: CO_2 output during rest subtracted from CO_2 output during flight. Muscle efficiency: ratio of total power output to aerodynamic power, under conditions where aerodynamic power is greater than inertial power. See text and Dickinson and Lighton (1995) for further explanation. Significant differences between lines are noted, where each value is compared to *wild type*. *n* = "fliers"/total number tested.
*$p < 0.01$.
#$p < 0.05$.
§$p < 0.001$.

differences exist between the phosphorylated and unphosphorylated cross-bridges, especially during oscillatory work output (stretch activation) where significant functional differences exist. Unfortunately, quick-freeze procedures that preserve dynamic structures for electron microscopy during the brief stretch-activated contractions of *Drosophila* flight muscle have not yet been developed to address these points.

Two-dimensional PAGE showed *Drosophila* IFM contains ~14 antigenically related isovariants of MLC2, 13 of which are phosphorylated in the adult IFM. One of the slow-migrating variants (spot P2a) co-localizes with spot 138 on the two-dimensional gels of *Drosophila* flight muscle proteins published by Mogami et al. (1982). However, in our gel system P2a usually resolves into six distinct spots. Two of the fast-migrating MLC2 isovariants (spots N1 and P1a) correspond to spots 148 and 149 of Mogami et al. (1982). Our results are consistent with those of Takano-Ohmuro et al. (1990), who showed that incubation of adult myosin with calf intestine alkaline phosphatase or potato acid phosphatase resulted in a substantial decrease in the number of myosin light chain isoforms.

Removal of the MLCK target serines produced changes in the level of nonphosphorylated versus phosphorylated variants, the largest occurring in $Mlc2^{S66A,S67A}$, in which the 3- to 10-fold increase in accumulation of the unphosphorylated variant was accompanied by a reduction or change in accumulation of the phosphorylated variants. The ratio of P1a to P1b was ~10 times higher in $Mlc2^{+}$ than in $Mlc2^{S66A,S67A}$, accompanied by a shift toward the basic end among slow-migrating phosphovariants.

Overall, the resulting pattern involved surprisingly small changes, especially in the accumulation of the unphosphorylated form of MLC2 compared to the total accumulation. Because serines 66 and 67 appear to be the only MLCK-dependent phosphorylatable residues, comparison of control and double mutant MLC2 gel spot densities suggest that ~5% of the native MLC2 protein density corresponds to the unphosphorylated variant, ~25% corresponds to the MLCK-dependent phosphorylated variants, and ~70% corresponds to variants whose residues are phosphorylated by kinase(s) other than MLCK.

Isometric tension versus calcium

The relationship between isometric tension in the flight muscle and calcium concentration was not affected by the serine substitutions (Fig. 3; Table 2), as reported previously (Tohtong et al., 1995). The maximal level of Ca^{2+}-activated tension in IFM of all strains (T_{max} ~2–3 kN/m^2) is exceptionally low compared to that of other striated muscle types, consistent with previous reports (Peckham et al., 1990; Tohtong et al., 1995). The similarity of isometric tensions between strains suggest that the impaired flight ability is not due to a marked alteration of calcium sensitivity or maximum tension in the IFM. However, the slope of the calcium-tension relationship, or Hill coefficient, was slightly less in the single serine mutants than in controls, a reduction that was either significant ($Mlc2^{S67A}$) or on the borderline of significance ($Mlc2^{S66A}$). Although MLCK-dependent phosphorylation may affect cross-bridge cooperativity [reflected in the Hill coefficient (Brenner, 1988)], the lack of pronounced differences in Hill coefficients among mutant lines suggests the effect is small at best in *Drosophila* IFM.

Cross-bridge recruitment and IFM power output depend on MLCK-dependent phosphorylation

Previous results (Tohtong et al., 1995) using skinned IFM fibers from $Mlc2^{S66A}$ and $Mlc2^{S66A,S67A}$ showed graded reductions in negative viscous moduli, work per oscillatory cycle, and power output. The frequency at which IFM oscillatory power is maximum (f_{max}) was not affected, except for $Mlc2^{S66A,S67A}$, where f_{max} was ~60% of control. To more directly assess cross-bridge function, we extracted cross-bridge kinetic parameters from the IFM complex stiffness data using a simple viscoelastic model of the sarcomere. This model consisted of one passive (A) and two active (B, C) viscoelastic components, represented by the Fourier terms $A(if/\alpha)^k$, $Bif/(b + if)$, and $Cif/(c + if)$, respectively (see Eq. 1 for definitions of model parameters).

The first term ($A(if/\alpha)^k$) approximates the frequency (f)-dependent complex stiffness of the IFM in the relaxed and rigor states. Relaxed and rigor frog skeletal muscle fibers also exhibit linear Nyquists of this kind (De Winkel et al., 1994), as do many substances with rubberlike elasticity (Machin, 1964). The second and third terms ($Bif/(b + if)$ and $Cif/(c + if)$) represent the complex stiffness of two frequency-dependent cross-bridge components (B and C). Since the imposed length perturbations were small (<0.25% of the sarcomere length, or <4 nm per half sarcomere), the viscoelastic properties represented by B and C are those of a steady-state population of cross-bridges undergoing relatively small fluctuations in strain about some mean position. Work is done on the apparatus (i.e., energy is transmitted to the apparatus) by synchronous activity of the cross-bridges over a range of frequencies, with maximum work performed by the cross-bridges at frequency b. Equivalent work is done on the cross-bridges (i.e., energy is transmitted to the cross-bridges) by the apparatus over a somewhat higher range of frequencies, with maximum work performed on the cross-bridges at frequency c. Process B represents de novo force production, and it underlies stretch activation (Zhao and Kawai, 1993). In the context of a simple 3-state cross-bridge scheme (Fig. 6), process B represents transitions between a weakly attached low (or zero)-force state (X_1) and a strongly attached, high-force state (X_2), with apparent rate constant $2\pi b$. Process C represents cross-bridge transitions between a state of high force maintenance (X_3) and the low-force state X_1, with apparent rate constant $2\pi c$. States X_1, X_2, and X_3 are assumed to be states in which myosin is bound to actin. Myosin in state X_1 is assumed to be in rapid equilibrium with myosin dissociated from actin (state X_0).

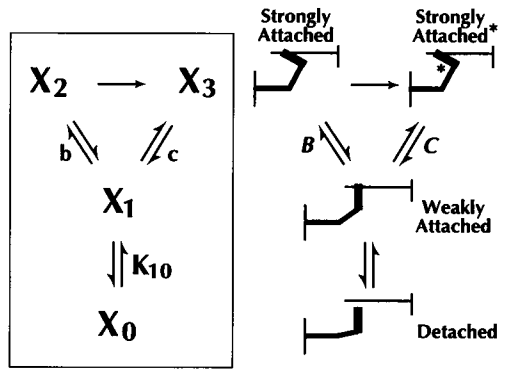

FIGURE 6 Three-state cross-bridge model. Process *B* defines transitions between a pre-force cross-bridge state (X_1) and a post-force state (X_2). Process *C* defines transitions between another post-force state (X_3) and state X_1. X_0 is a state in which the myosin head is fully detached from actin. The cross-bridge states incorporate MgATP binding, MgATP hydrolysis, or release of phosphate and MgADP (Maughan et al., 1994). Roughly speaking, process *B* can be viewed as cross-bridge attachment and de novo force generation; process *C*, as cross-bridge detachment and force abolishment. The proposed MLCK-phosphorylation dependent recruitment of power-generating cross-bridges is indicated as a phosphorylation-dependent change in equilibrium constant (K_{10}) determining the ratio of X_1 to X_0. See text for further explanation.

For length perturbations of $\Delta L/L$ (equivalent to 0.00125 in the present study) the maximum power generated by the cross-bridges in the IFM (P_B) is equal to π b B $(\Delta L/L)^2$ (Tohtong et al., 1995). Thus P_B, which depends strongly on the total number of interacting (recruited) cross-bridges, is an index of the power capacity of the IFM. P_B was sharply reduced in $Mlc2^{S66A}$ and $Mlc2^{S66A,S67A}$ compared with control, with $Mlc2^{S66A,S67A}$ exhibiting the lowest value (P_B; Table 3). The reduced values of P_B can explain the corresponding reductions in net power of the IFM (P_{IFM}; Table 3).

The amplitudes of processes *B* and *C* were significantly reduced in $Mlc2^{S66A}$ and $Mlc2^{S66A,S67A}$ compared with controls (*B* and *C*, Table 3). In contrast, characteristic frequencies *b* and *c* of the mutants were not significantly different than those of the controls (Table 3). This result supports our earlier hypothesis (Tohtong et al., 1995) that the cross-bridge kinetics are not significantly affected by removal of the MLCK-dependent phosphorylation sites. It is unlikely that the cross-bridge unitary stiffness or force was altered because maximum steady-state isometric tension was not significantly different between fly lines. Because B is proportional to the number of cross-bridges undergoing the transition between states X_1 and X_2, the simplest interpretation of our results is that phosphorylation site removal increases the number of detached heads (state X_0), thereby reducing the number of weakly attached heads (state X_1) that can undergo a power stroke. Likewise, C is proportional to the number of cross-bridges undergoing the transition from strongly (X_3) to a weakly (X_1) bound states. The fact that C is reduced by about the same amount as B is consistent with a reduction in number of attached cross-bridges due to removal of the phosphorylation site. Since the basal level of isometric tension generated by Ca^{2+} activation is unaffected, phosphorylation site removal only reduces the number of additional cross-bridges formed during stretch that contribute to force generation.

Alteration of in vivo power output

After tethering, some flies from the phosphorylation-site mutant strains could not achieve sustained flights, although they could generate at least a few oscillatory wingstrokes. Like the majority, they exhibited a stereotyped flight initiation reflex upon removal of their tarsal substrate, but then produced only a few low-amplitude wingstrokes before stopping. $Mlc2^{S66A,S67A}$ yielded the fewest fliers (Table 4), corroborating the results using the Sparrow box (Table 1). The individuals that were capable of sustained flight behavior provided a means of quantifying the effects of the MLC2 alterations on power production and flight performance.

Although the values of maximum flight force and maximum mechanical power were lower among the mutants that could fly, most of these animals could generate enough power and lift to support body weight (Table 4). In $Mlc2^{S66A}$ and $Mlc2^{S66A,S67A}$, the stroke frequency during hovering flight was significantly below wild-type. These flies appear to compensate for a reduced cross-bridge number and lower wingbeat frequency by elevating stroke amplitude (and presumably muscle strain). In $Mlc2^{S67A}$, however, little if any compensation is required since the number of recruited cross-bridges is similar to that of wild type. Altogether, these results illustrate the direct voluntary control over both the frequency and amplitude of the IFM contractions via 17 pairs of synchronous steering muscles which actively alter the mechanics of the thorax and wing hinge (Dickinson and Tu, 1997). These tiny muscles presumably allow the mutant flies to compensate for a lower than normal stroke frequency by elevating stroke amplitude, thus producing enough power and force to sustain body weight.

Alterations of MLC2 resulted in a decrease in the maximum metabolic rate (metabolic power output) in the flight arena, as measured by CO_2 respiration (Table 4). Maximum metabolic rate was ~80% of wild-type and control values in the double substitution line ($Mlc2^{S66A,S67A}$), and ~70% in the single substitutions lines ($Mlc2^{S66A}$ and $Mlc2^{S67A}$, respectively). The metabolic rate during flight is roughly 10 times that during rest, an increase that must result almost entirely from the activity of the flight muscles. Thus, the decrease in the metabolic rate of the mutant flies can be attributed to an attenuation of the power output of the IFM. Because we did not make a quantitative measurement of muscle mass in each individual, we cannot completely exclude the possibility that some of the differences in the performance of mutant and control flies was due to differences in the relative size of the IFM in different lines. However, the similarity of fiber diameters among strains, measured during the in vitro analysis of isolated fibers,

support the notion that differences among lines result from physiological alterations associated with the mutations rather than from effects due to differences in muscle mass.

The metabolic rate of any muscle is equal to mechanical power divided by mechanical efficiency. In the case of IFM in all mutant flies, the drop in maximum metabolic rate was caused by a decrease in mechanical power and not by an increase in muscle efficiency (Table 4). Muscle efficiency in mutant, wild-type, and control lines was ~10%, which is consistent with previously reported values (Dickinson and Lighton, 1995; Lehmann and Dickinson, 1997).

Possible mechanism of phosphorylation-dependent power enhancement

In vertebrate striated muscle, MLCK-dependent myosin regulatory light chain phosphorylation appears to either shift mass (i.e., move myosin heads) away from the thick filament backbone (Barany et al., 1979; Metzger et al., 1989; Sweeney et al., 1994) or to spread mass (i.e., disorder the heads) about the thick filament backbone (Craig et al., 1987; Levine et al., 1991). These structural changes probably reflect increased mobility of the myosin heads, and they likely underlie the MLCK-dependent phosphorylation effect on Ca^{2+} sensitivity and enhanced rate of force production reported for vertebrate muscle (Sweeney and Stull, 1986, 1990; Metzger et al., 1989). Poetter et al. (1996), in explaining the effects of inherited mutations of the regulatory light chain of human heart and skeletal muscle, speculate that phosphorylation of the serines may modify the regional elasticity of the myosin neck (the elongated region that includes the 20-kD α-helix and the attached regulatory and essential light chains). As mentioned in the Introduction, sinusoidal perturbations of the cross-bridges are thought to alter at least one strain-sensitive rate constant (Thorson and White, 1983; Zhao and Kawai, 1993), thereby increasing force during oscillatory contractions. If part or all of the strain sensitivity of *Drosophila* myosin originates in the neck region, it is possible that removal of the MLCK-dependent phosphorylation sites on MLC2 diminishes oscillatory power output by altering neck compliance. This possibility cannot be excluded, given the amino acid sequence homology between *Drosophila* and vertebrate regulatory light chains over their main portions.

However, the presence of the unique N-terminal extension in *Drosophila* MLC2 suggests an additional mechanism by which power production can be increased by phosphorylation. The N-terminal extension has the appropriate amino acid residues to interact electrostatically with charged residues flanking the MLCK substrate serines in the absence of MLCK-dependent phosphorylation. It is possible that phosphorylation of Ser-66 and Ser-67 could relieve the putative interaction and allow the folded N-terminal extension to extend and link with actin or the IFM-specific tropomyosin isoform, TnH, thereby increasing the probability the head binds to actin (Tohtong et al., 1995). In the context of the 3-state model of Fig. 6, the functional expression of this link (and an explanation of cross-bridge recruitment) would be a phosphorylation-dependent increase in equilibrium constant K_{10} that reflects an increased probability of myosin head attachment (i.e., increased number of cross-bridges in state X_1 and reduced number in state X_0). The results of Table 3 suggest that this increase is ~2.5-fold (the ratio B of $Mlc2^{+}$ to B of $Mlc^{S66A,S67A}$; i.e., 412 kN m^{-2}/166 kN m^{-2}). The stiffness of the putative MCL2/thin filament link might contribute significantly to the passive stiffness of the IFM. It is possible the reduced value of A (the coefficient of passive viscoelasticity) in $Mcl2^{S66A}$ and $Mlc2^{S66A,S67A}$ (Table 3) reflects a reduced number of putative links in the absence of phosphorylated serines. However, the normal ultrastructure supports the hypothesis that some dynamic property of cross-bridge complex formation is affected by the mutation, and that phosphorylation-induced changes in the dynamic properties of cross-bridge function are responsible for the defects in power production in the mutants.

The authors are grateful to Joe Haeberle, Masataka Kawai, and Justin Molloy for their help in the initial stages of this research. We also thank William Barnes, Janet Hurley, Clifford Beall, and Michael Reedy for assistance and advice.

This study was supported by the National Institutes of Health Grant RO1 AR40234 (to D.M.).

REFERENCES

Abbott, R. H., and G. J. Steiger. 1977. Temperature and amplitude dependence of tension transients in glycerinated skeletal and insect fibrillar muscle. *J. Physiol.* 266:13–42.

Barany, K., M. Barany, J. M. Gillis, and M. J. Kushmerick. 1979. Phosphorylation-dephosphorylation of the 18,000-dalton light chain of myosin during the contraction-relaxation cycle of frog muscle. *J. Biol. Chem.* 254:3617–3623.

Brenner, B. 1988. Effect of cross-bridge turnover kinetics in skinned single rabbit psoas fibers: implications for regulation of muscle contraction. *Proc. Natl. Acad. Sci. USA.* 85:3265–3269.

Bullard, B. 1983. Contractile proteins of insect flight muscle. *TIBS.* 8: 68–70.

Bullard, B., K. Leonard, A. Larkins, G. Butcher, C. Karlik, and E. Fyrberg. 1988. Troponin of asynchronous flight muscle. *J. Mol. Biol.* 204: 621–637.

Craig, R., R. Padron, and J. Kendrick-Jones. 1987. Structural changes accompanying phosphorylation of tarantula muscle myosin filaments. *J. Cell Biol.* 105:1319–1327.

David, C. T. 1978. The relationship between body angle and flight speed in free flying *Drosophila. Physiological Entomology.* 3:191–195.

De Winkel, M. E. M., T. Blangé, and B. W. Treijtel. 1994. High frequency characteristics of elasticity of skeletal muscle fibres kept in relaxed and rigor state. *J. Muscle Res. Cell Motil.* 15:130–144.

Dickinson, M. H., and K. G. Gotz. 1996. The wake dynamics and flight forces of the fruit fly, *Drosophila melanogaster. J. Exp. Biol.* 2085–2104.

Dickinson, M. H., and J. R. B. Lighton. 1995. Muscle efficiency and elastic storage in the flight motor of *Drosophila melanogaster. Science.* 128: 87–89.

Dickinson, M. H., and M. S. Tu. 1997. The function of *Dipteran* flight muscle. *Comp. Biochem. Physiol.* 116A:223–238.

Drummond, D. R., E. S. Hennessey, and J. C. Sparrow. 1991. Characterization of missense mutations in the *Act88F* gene of *Drosophila melanogaster. Mol. Gen. Genet.* 226:70–80.

Eisenberg, E., and L. E. Greene. 1980. The relation of muscle biochemistry to muscle physiology. *Annu. Rev. Physiol.* 42:293–309.

Ellington, C. P. 1984. The aerodynamics of insect flight. VI. Lift and power requirements. *Phil. Trans. R. Soc. Lond. B.* 305:145–181.

Gilmour, K. M., and C. P. Ellington. 1993. Power output of glycerinated bumblebee flight muscle. *J. Exp. Biol.* 183:77–100.

Godt, R. E., and B. D. Lindley. 1982. Influence of temperature upon contractile activation and isometric force production in mechanically skinned muscle fibers of the frog. *J. Gen. Physiol.* 80:279–297.

Gotz, K. G. 1987. Course-control, metabolism and wing interference during ultralong tethered flight in *Drosophila melanogaster*. *J. Exp. Biol.* 128:35–46.

Gotz, K. G., and U. Wandel. 1984. Optomotor control of the force of flight in *Drosophila* and *Musca* II. Covariance of lift and thrust in still air. *Biol. Cybernetics.* 51:135–139.

Granzier, H. L. M., and K. Wang. 1993a. Passive tension and stiffness of vertebrate skeletal and insect flight muscles: The contribution of weak cross-bridges and elastic filaments. *Biophys. J.* 65:2141–2159.

Granzier, H. L. M., and K. Wang. 1993b. Interplay between passive tension and strong and weak binding cross-bridges in insect indirect flight muscle: a functional dissection by gelsolin-mediated thin filament removal. *J. Gen. Physiol.* 101:235–270.

Hyatt, C. J., and D. W. Maughan. 1994. Fourier analysis of wingbeat signals: assessing the effects of genetic alterations of flight muscle structure in *Diptera*. *Biophys. J.* 67:1149–1154.

Jewell, B. R., and J. C. Ruegg. 1966. Oscillatory contraction of insect fibrillar muscle after glycerol extraction. *Proc. Roy. Soc.* 164:428–459.

Kawai, M., and P. W. Brandt. 1980. Sinusoidal analysis: a high resolution method for correlating biochemical reactions with physiological processes in activated skeletal muscle of rabbit, frog and crayfish. *J. Muscle Res. Cell Motil.* 1:279–303.

Kawai, M., Y. Saeki, and Y. Zhao. 1993. Crossbridge scheme and the kinetic constants of elementary steps deduced from chemically skinned papillary and trabecular muscles of the ferret. *Circ. Res.* 73:35–50.

Kunkle, T. A., J. D. Roberts, and R. A. Zakour. 1987. Rapid and efficient site-specific mutagenesis without phenotypic selection. *Methods Enzymol.* 154:367–382.

Lehmann, F.-O., and M. H. Dickinson. 1997. The changes in power requirements and muscle efficiency during elevated force production in the fruit fly, *Drosophila melanogaster*. *J. Exp. Biol.* 200:1133–1143.

Levine, R. J. C., P. D. Chantler, R. W. Kensler, and J. L. Woodhead. 1991. Effects of phosphorylation by myosin light chain kinase on the structure of *Limulus* thick filaments. *J. Cell Biol.* 113:563–572.

Lighton, J. R. B. 1991. Measurement of insect metabolism. *In* Concise Encyclopedia of Biological and Biomedical Measurement Systems. P. A. Payne, editor. Pergamon, New York. 201–208.

Machin, K. E. 1964. Feedback theory and its application to biological systems. *Symp. Soc. Exp. Biol.* 18:421–445.

Matsuda, G., Y. Suzuyama, T. Maita, and T. Umegane. 1977. The L-2 light chain of chicken skeletal muscle myosin. *FEBS Lett.* 84:53–56.

Maughan, D. W., and R. E. Godt. 1989. Equilibrium distribution of ions in a muscle fiber. *Biophys. J.* 56:717–722.

Maughan, D., H. Yamashita, and C. Hyatt. 1994. Effects of MgATP, MgADP, and phosphate on complex stiffness moduli of skinned flight muscle fibers of *Drosophila*. *Biophys. J.* 66:303*a*. (Abstr.).

Metzger, J. M., M. L. Greaser, and R. L. Moss. 1989. Variations in cross-bridge attachment rate and tension with phosphorylation of myosin in mammalian skinned skeletal muscle fibers: implications for twitch potentiation in intact muscle. *J. Gen. Physiol.* 93:855–883.

Mogami, K., S. C. Fugita, and Y. Hotta. 1982. Identification of *Drosophila* indirect flight muscle myofibrillar proteins by means of two-dimensional electrophoresis. *J. Biochem.* 91:643–650.

O'Farrell, P. H. 1975. High resolution two-dimensional electrophoresis of proteins. *J. Biol. Chem.* 250:4007–4021.

Parker, V. P., S. Falkenthal, and N. Davidson. 1985. Characterization of the myosin light-chain-2 gene of *Drosophila melanogaster*. *Mol. Cell. Biol.* 5:3058–3068.

Peckham, M., J. E. Molloy, J. C. Sparrow, and D. C. S. White. 1990. Physiological properties of the dorsal longitudinal flight muscle and tergal depressor of the trochanter muscle of *Drosophila melanogaster*. *J. Muscle Res. Cell Motil.* 11:203–215.

Poetter, K., H. Jiang, S. Hassanzadeh, S. R. Master, A. Chang, M. C. Dalakas, I. Rayment, J. R. Sellers, L. Fananapazir, and N. D. Epstein. 1996. Mutations in either the essential or regulatory light chains of myosin are associated with a rare myopathy in human heart and skeletal muscle. *Nat. Genet.* 13:63–69.

Pringle, J. W. S. 1949. The excitation and contraction of the flight muscles of insects. *J. Physiol.* 108:226–232.

Reedy, M. C., M. K. Reedy, K. R. Leonard, and B. Bullard. 1994. Gold/Fab immunoelectron microscopy localization of troponin H and troponin T in *Lethocerus* flight muscle. *J. Mol. Biol.* 239:52–67.

Saide, J. S., S. Chin-Bow, J. Hogan-Sheldon, L. Busquets-Turner, J. O. Vigoreaux, K. Valgeirsdottir, and M. L. Pardue. 1989. Characterization of components of Z-bands in the fibrillar flight muscle of *Drosophila melanogaster*. *J. Cell Biol.* 109:2157–2167.

Squire, J. M. 1992. Muscle filament lattices and stretch-activation: the match-mismatch model reassessed. *J. Muscle Res. Cell Motil.* 13: 183–189.

Steiger, G. J. 1977. Stretch activation and tension transients in cardiac, skeletal and insect flight muscle. *In* Insect Flight Muscle. R. T. Tregear, editor. Elsevier–North Holland Biomedical Press, Amsterdam. 221–268.

Sweeney, H. L., and J. T. Stull. 1986. Phosphorylation of myosin in permeabilized mammalian cardiac and skeletal muscle cells. *Am. J. Physiol.* 250:C657–C660.

Sweeney, H. L., and J. T. Stull. 1990. Alteration of cross-bridge kinetics by myosin light chain phosphorylation in rabbit skeletal muscle: implications for regulation of actin-myosin interaction. *Proc. Natl. Acad. Sci. USA.* 87:414–418.

Sweeney, H. L., Z. Yang, G. Zhi, J. T. Stull, and K. M. Trybus. 1994. Charge replacement near the phosphorylatable serine of the myosin regulatory light chain mimics aspects of phosphorylation. *Proc. Natl. Acad. Sci. USA.* 91:1490–1494.

Takano-Ohmuro, H., S. Takahashi, G. Hirose, and K. Maruyama. 1990. Phosphorylated and dephosphorylated myosin light chains of *Drosophila* fly and larva. *Comp. Biochem. Physiol.* 95B:171–177.

Tawada, K., and M. Kawai. 1990. Covalent cross-linking of single fibers from rabbit psoas increases oscillatory power. *Biophys. J.* 57:643–647.

Thorson, J., and D. C. S. White. 1983. Role of cross-bridge distortion in the small-signal mechanical dynamics of insect and rabbit striated muscle. *J. Physiol.* 343:59–84.

Toffenetti, J., D. Mischke, and M. L. Pardue. 1987. Isolation and characterization of the gene for myosin light chain two of *Drosophila melanogaster*. *J. Cell Biol.* 104:19–28.

Tohtong, R., H. Yamashita, M. Graham, J. Haeberle, A. Simcox, and D. Maughan. 1995. Impairment of muscle function caused by mutations of phosphorylation sites in myosin regulatory light chain. *Nature.* 374: 650–653.

Vigoreaux, J. O., and L. M. Perry. 1994. Multiple isoelectric variants of flightin in Drosophila stretch-activated muscles are generated by temporally regulated phosphorylations. *J. Muscle Res. Cell Motil.* 15: 607–616.

Vigoreaux, J. O., J. S. Saide, K. Valgeirsdottir, and M. L. Pardue. 1993. Flightin, a novel myofibrillar protein of *Drosophila* stretch-activated muscles. *J. Cell Biol.* 121:587–598.

Warmke, J., M. Yamakawa, J. E. Molloy, S. Falkenthal, and D. W. Maughan. 1992. A myosin light chain-2 mutation affects flight, wingbeat frequency and indirect flight muscle contraction kinetics in *Drosophila*. *J. Cell Biol.* 119:1523–1536.

Weis-Fogh, T. 1973. Quick estimates of flight fitness in hovering animals, including novel mechanisms for lift production. *J. Exp. Biol.* 59: 169–230.

Wray, J. S. 1979. Filament geometry and the activation of insect flight muscle. *Nature.* 280:325–326.

Zhao, Y., and M. Kawai. 1993. The effect of lattice spacing change on cross-bridge kinetics in chemically skinned rabbit psoas muscle fibers. II. Elementary steps affected by the spacing change. *Biophys. J.* 64: 197–210.

Zhao, Y., and M. Kawai. 1994. BDM affects nucleotide binding and force generation steps of the cross-bridge cycle in rabbit psoas muscle fibers. *Am. J. Physiol.* 266:C437–C447.